Inorganic Chemistry

pubs.acs.org/IC Article

Involvement of 5f Orbitals in the Covalent Bonding between the Uranyl Ion and Trialkyl Phosphine Oxide: Unraveled by Oxygen K-Edge X-ray Absorption Spectroscopy and Density Functional Theory

Yusheng Zhang, Wuhua Duan, Yuning Yang, Tian Jian, Yusen Qiao, Guoxi Ren, Nian Zhang, Lei Zheng, Wensheng Yan, Jianchen Wang, Jing Chen, Stefan G. Minasian, and Taoxiang Sun*

Cite This: https://doi.org/10.1021/acs.inorgchem.1c02236 Read Online

ABSTRACT: Monodentate organophosphorus ligands have been used for the extraction of the uranyl ion (UO_2^{2+}) for over half a century and have exhibited exceptional extractability and selectivity toward the uranyl ion due to the presence of the phosphoryl group (O═P). Tributyl phosphate (TBP) is the extractant of the world-renowned PUREX process, which selectively recovers uranium from spent nuclear fuel. Trialkyl phosphine oxide (TRPO) shows extractability toward the uranyl ion that far exceeds that for other metal ions, and it has been used in the TRPO process. To date, however, the mechanism of the high affinity of the phosphoryl group for UO_2^{2+} remains elusive. We herein investigate the bonding covalency in a series of complexes of UO_2^{2+} with TRPO by oxygen K-edge X-ray absorption spectroscopy (XAS) in combination with density functional theory (DFT) calculations. Four TRPO ligands with different R substituents are examined in this work, for which both the ligands and their uranyl complexes are crystallized and investigated. The study of the electronic structure of the TRPO ligands reveals that the two TRPO molecules, irrespective of their substituents, can engage in σ- and π-type interactions with U 5f and 6d orbitals in the $UO_2Cl_2(TRPO)_2$ complexes. Although both the axial (O_{yl}) and equatorial (O_{eq}) oxygen atoms in the $UO_2Cl_2(TRPO)_2$ complexes contribute to the X-ray absorption, the first pre-edge feature in the O K-edge XAS with a small intensity is exclusively contributed by O_{eq} and is assigned to the transition from O_{eq} 1s orbitals to the unoccupied molecular orbitals of $1b_{1u} + 1b_{2u} + 1b_{3u}$ symmetries resulting from the σ- and π-type mixing between U 5f and O_{eq} 2p orbitals. The small intensity in the experimental spectra is consistent with the small amount of O_{eq} 2p character in these orbitals for the four $UO_2Cl_2(TRPO)_2$ complexes as obtained by Mulliken population analysis. The DFT calculations demonstrate that the U 6d orbitals are also involved in the U−TRPO bonding interactions in the $UO_2Cl_2(TRPO)_2$ complexes. The covalent bonding interactions between TRPO and UO_2^{2+}, especially the contributions from U 5f orbitals, while appearing to be small, are sufficiently responsible for the exceptional extractability and selectivity of monodentate organophosphorus ligands for the uranyl ion. Our results provide valuable insight into the fundamental actinide chemistry and are expected to directly guide actinide separation schemes needed for the development of advanced nuclear fuel cycle technologies.

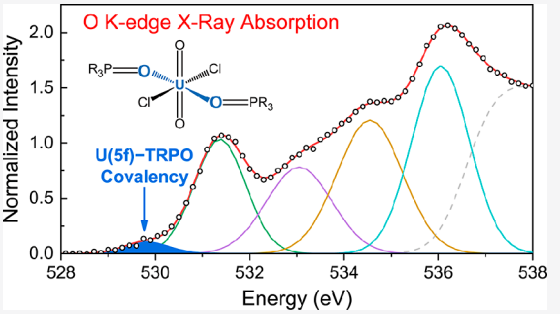

INTRODUCTION

Extraction separation of the uranyl ion (UO_2^{2+}) is of great significance for the efficient utilization of uranium resources and thus the sustainable development of nuclear energy.[1−4] A number of ligands have been adopted for the extraction of UO_2^{2+}, among which the monodentate organophosphorus extractants display prominent extractability and selectivity.[1,5] For example, tributyl phosphate (TBP) is the extractant of the world-renowned PUREX process to recover UO_2^{2+} from spent nuclear fuel.[1] Another example is trialkyl phosphine oxide (TRPO), which shows higher extractability for UO_2^{2+} than does TBP. The TRPO ligands are used as extractants in the TRPO process, recovering the uranyl ion and other actinides from high-level liquid waste.[6] In the TRPO process, the distribution ratio of UO_2^{2+} far exceeds that for other metal ions.[6] The interactions of the phosphoryl group (O═P) in these ligands with UO_2^{2+} are considered to be responsible to the extraordinary extractability and selectivity and have been investigated by crystallography and theoretical calculations over the past several decades.[7−18] The crystal structures suggest the coordination of the oxygen atoms in the

Received: July 26, 2021

https://doi.org/10.1021/acs.inorgchem.1c02236
Inorg. Chem. XXXX, XXX, XXX−XXX

phosphoryl group with UO_2^{2+}. The theoretical calculations provide the geometry of the complexes and the binding energies between TRPO and UO_2^{2+}, and the bonding order analysis indicates the ionic bonding properties between UO_2^{2+} and the phosphoryl group.[16−18] These studies are, however, insufficient to account for the high extractability and selectivity of the monodentate organophosphorus extractants for UO_2^{2+}, and its underlying mechanism requires further investigation.

The most significant character that distinguishes uranium from transition metals and lanthanides is the presence of 5f and 6d orbitals. The involvement of both 5f and 6d orbitals in the covalent bonds between uranium and axial oxygen (O_{yl}) atoms induces a geometrically linear and redox-stable uranyl ion,[19−22] around which other ligands are confined to the equatorial plane. Exploring the coordination behavior between the uranyl ion and the equatorial ligands is an essential issue of current interest because of the direct relevance to the extraction behavior of extractants.[23−26] Indications are gradually emerging that the selectivity of extractants toward specific metal ions is related to their covalent bonding interactions.[27,28] Given the great involvement of the U 5f orbitals in chemical bonding,[20,21] we hypothesized that covalency in the bonding interaction between the uranyl ion and the O-donor from the phosphoryl group, U−(O═P), may be partially responsible for the remarkable extractability and selectivity of the monodentate organophosphorus extractants for the uranyl ion.

As one of the most versatile and direct spectroscopic techniques in the evaluation of the bonding covalency in d and f block compounds, ligand K-edge X-ray absorption spectroscopy (XAS) in combination with density functional theory (DFT) and time-dependent DFT (TDDFT) calculations have attracted much attention in the past decades.[29−47] The ligand K-edge XAS probes the transition from the ligand 1s orbitals to unoccupied molecular orbitals (MOs) containing ligand p character. This technique can quantify the component of ligand p character in the metal d and f orbitals, hence the covalency of the metal−ligand bond.[29] To guide the interpretation of the XAS spectra, DFT can manifest the orbital energy levels and orbital compositions, which are related to the transition energies and intensities, respectively. TDDFT can simulate the XAS spectra to compare with the experimental spectra. XAS and DFT/TDDFT in combination have been implemented to reveal the covalent bonding behavior of the f and d orbitals of lanthanides and actinides upon mixing with p orbitals of ligands.[33−47]

Our goal in this work is to provide insight into the contributions of U 6d and especially 5f orbitals to chemical bonding covalency between UO_2^{2+} and phosphoryl group, thereby revealing the mechanism of the remarkable extractability and selectivity of the monodentate organophosphorus extractants for UO_2^{2+}. Complexes of TBP and UO_2^{2+} cannot be isolated as pure crystalline materials with high symmetry that is desirable for spectroscopic analysis.[48−50] To overcome this challenge, we have tested four different TRPO ligands (Scheme 1), and obtained the single crystals of both the ligands and the uranyl complexes, including triphenyl phosphine oxide (TPPO), cyclohexyldiphenyl phosphine oxide (CDPPO), ethyldiphenyl phosphine oxide (EDPPO), and tricyclohexyl phosphine oxide (TCyPO). These four ligands have demonstrated excellent extraction and separation performance toward the uranyl ion (Figure S1). Elementary covalent interactions between UO_2^{2+} and TRPO in the entire series of $UO_2Cl_2(TRPO)_2$ complexes are examined using oxygen K-edge XAS, with the interpretation guided by DFT/TDDFT calculations. This allows us to examine the electronic structures of both the TRPO ligands and the $UO_2Cl_2(TRPO)_2$ complexes as well as the effect of the R substituents of the TRPO ligands on their interactions with the uranyl ion.

Scheme 1. Molecular Structures of the Ligands Used in the Present Work

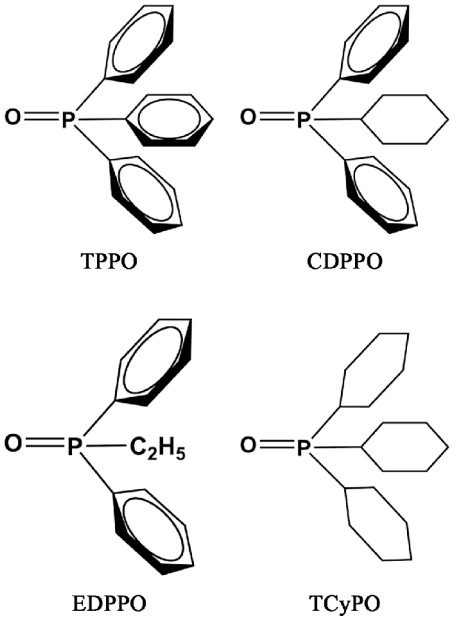

RESULTS AND DISCUSSION

Sample Preparation. All the TRPO and $UO_2Cl_2(TRPO)_2$ complexes studied in this work were prepared in large quantities, isolated as highly pure crystalline solids, and characterized by single-crystal X-ray diffraction prior to use.[7−13,51−59] Chloride is employed as the counterion in the $UO_2Cl_2(TRPO)_2$ complexes to avoid the interference of the oxygen-containing anions such as nitrate to the O K-edge XAS spectra. All the crystal structures of TRPO and $UO_2Cl_2(TRPO)_2$ obtained in this work are illustrated in Figure 1. Data collection and refinement details are available in Tables S1 and S2. Some of the TRPO ligands and $UO_2Cl_2(TRPO)_2$ complexes have been reported previously;[7−13,51−59] however, to the best of our knowledge, the crystal structures of CDPPO, $UO_2Cl_2(CDPPO)_2$, and $UO_2Cl_2(EDPPO)_2$ have not been reported. The P═O bond length varies from 1.487 to 1.493 Å in TRPO (Table S3), and these values increase to about 1.519 Å in the $UO_2Cl_2(TRPO)_2$ complexes (Table S4), suggesting the bonding interaction between the TRPO ligands and the uranyl ion. The two TRPO ligands are trans to each other in all the $UO_2Cl_2(TRPO)_2$ complexes, maintaining the complexes in C_i symmetry. The U−O_{eq} bond length is in the range of 2.288−2.307 Å, much longer than the U−O_{yl} bond length (1.762−1.769 Å). The distances between uranium and axial oxygen (O_{yl}) as well as those between uranium and the oxygen of TRPO in the equatorial plane (O_{eq}) show no apparent difference in the four $UO_2Cl_2(TRPO)_2$ complexes. On the basis of this analysis of the geometric data obtained by X-ray crystallography, changing the substituents in TRPO has no evident effect on the bonding interaction with the uranyl ion.

https://doi.org/10.1021/acs.inorgchem.1c02236
Inorg. Chem. XXXX, XXX, XXX−XXX

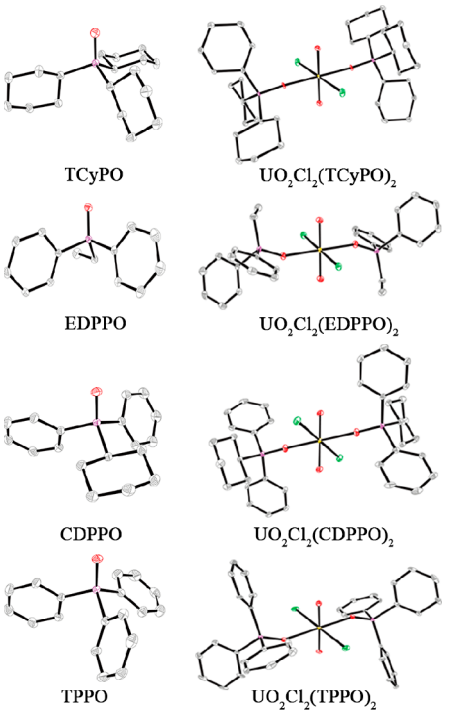

Figure 1. Crystal structures of TRPO and $UO_2Cl_2(TRPO)_2$ investigated in this work with thermal ellipsoids drawn at the 30% probability level. Hydrogen atoms have been omitted for clarity. Oxygen, phosphorus, carbon, chloride, and uranium atoms are in red, purple, white, green, and yellow, respectively.

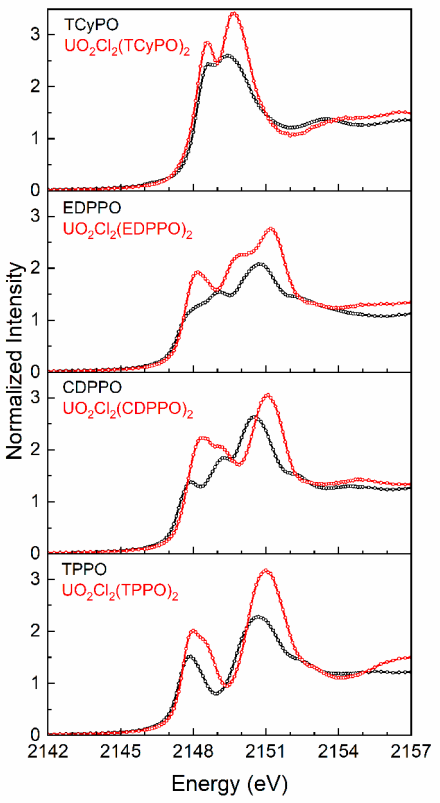

Figure 2. Background-subtracted and normalized P K-edge XAS spectra for the free ligands TRPO (black) and their uranyl complexes $UO_2Cl_2(TRPO)_2$ (red).

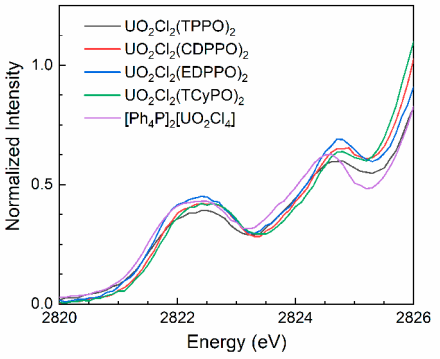

Figure 3. Background-subtracted and normalized Cl K-edge XAS spectra for the $UO_2Cl_2(TRPO)_2$ complexes in comparison with that for $[Ph_4P]_2[UO_2Cl_4]$. For curve-fitting analysis, refer to Figure S6.

P and Cl K-Edge XAS. Spectra at the P and Cl K-edges were measured initially to probe electronic structure from the perspective of heavier atoms in the coordination sphere. Previous studies have shown that P or Cl K-edge XAS can be sensitive to bonding with phosphine or chloride ligands directly bound to metal centers.[33−39,60−65] Figure 2 shows the background-subtracted and normalized P K-edge XAS spectra for the free ligands TRPO and their uranyl complexes $UO_2Cl_2(TRPO)_2$. In the P K-edge XAS of the TRPO series, the pre-edge features show substantial differences with the variation of the R substituents. A pre-edge feature around 2147.8 eV is observed in the spectrum of TPPO, CDPPO, and EDPPO, and this feature disappears in the spectrum of TCyPO. Peak shift and transition intensity variations are observed when comparing the P K-edge XAS of $UO_2Cl_2(TRPO)_2$ with that of TRPO, indicating the change of the electron distribution on the phosphorus atoms, and thus the bonding interaction between TRPO and the uranyl ion in the $UO_2Cl_2(TRPO)_2$ complexes.

Spectra at the Cl K-edge were measured to probe changes in electronic structure from the perspective of the chloride ligands in the $UO_2Cl_2(TRPO)_2$ complexes (Figure 3). The spectra are similar to that previously reported for $[Ph_4P]_2[UO_2Cl_4]$,[37] in that closely spaced pre-edge features are observed at 2822.4 and 2824.8 eV for all complexes. Previous DFT analyses for $[Ph_4P]_2[UO_2Cl_4]$ indicated that these features arise from transitions between the Cl 1s orbitals to the unoccupied MOs of $1b_{1u} + 1b_{2u} + 1b_{3u} + 2b_{2u}$ and $1b_{1g}$ symmetries, respectively.[37] The close correspondence between the Cl K-edge spectra for $[Ph_4P]_2[UO_2Cl_4]$ and each of the $UO_2Cl_2(TRPO)_2$ complexes indicates that the interactions of Cl 3p orbitals with the U 5f and 6d orbitals are not significantly perturbed when varying the other equatorial ligands.

O K-edge XAS. Since the P and Cl K-edge XAS measurements only provided indirect probes of the U−O bonds, we sought additional insights using O K-edge XAS. The O K-edge XAS data were collected by total fluorescence yield (TFY) detection for both TRPO and the $UO_2Cl_2(TRPO)_2$ complexes. The background-subtracted and normalized O K-edge XAS are shown in Figure 4. In the TRPO series, the pre-edge features show substantial differences with the variation of the R substituents. A substantial pre-edge transition around 532 eV is observed in the spectrum of TPPO, which is diminished in the spectra of CDPPO and EDPPO. For

https://doi.org/10.1021/acs.inorgchem.1c02236
Inorg. Chem. XXXX, XXX, XXX−XXX

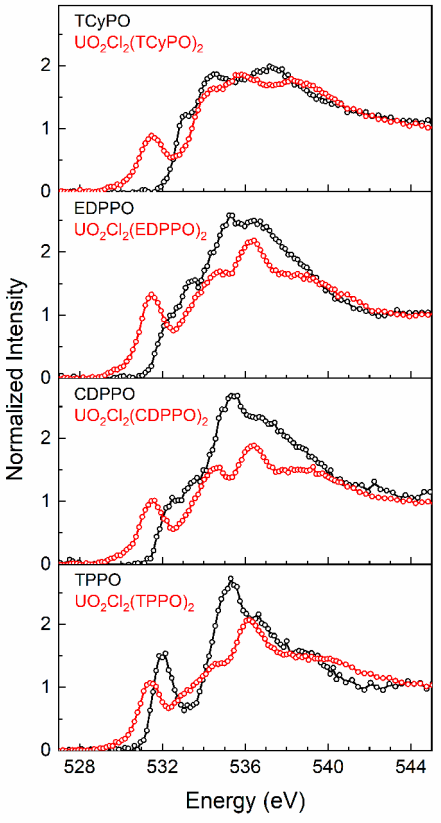

Figure 4. Background-subtracted and normalized O K-edge XAS spectra for the free ligands TRPO (black) and their uranyl complexes $UO_2Cl_2(TRPO)_2$ (red).

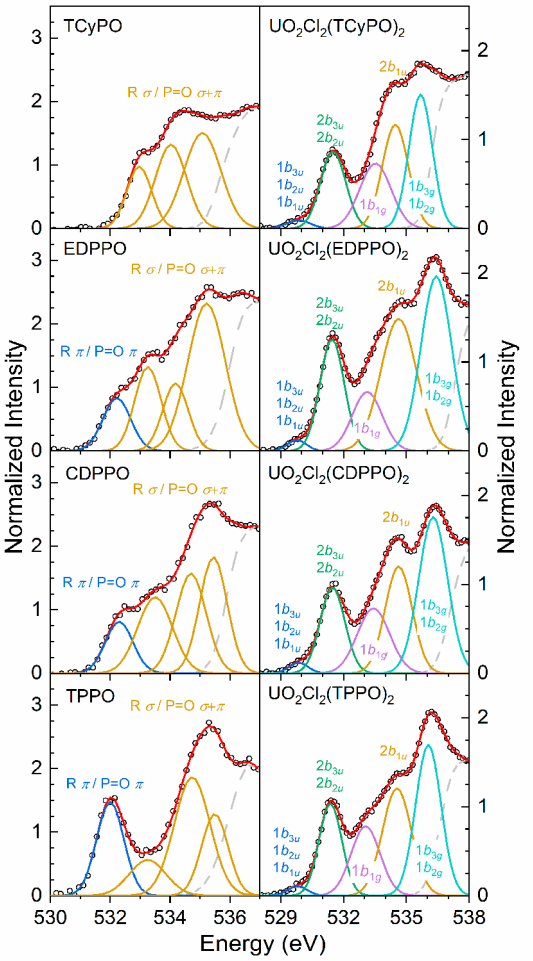

Figure 5. Curve-fitting results for O K-edge XAS for TRPO (left) and $UO_2Cl_2(TRPO)_2$ (right). The experimental data are shown in black circles, and the total curve fits are shown in red traces. Postedge residuals (dashed gray traces) are generated by subtracting the pre-edge Gaussian functions (blue, yellow, green, purple, and light blue) from the total curve fits.

TCyPO, no transition at 532 eV is observed in the O K-edge XAS. All the $UO_2Cl_2(TRPO)_2$ complexes display similar pre-edge features in the O K-edge spectra, with a distinct pre-edge feature near 531.5 eV and a small shoulder feature around 530 eV. One can see from Figure 4 that the onset of the pre-edge XAS for all the $UO_2Cl_2(TRPO)_2$ complexes moves to lower energy as compared with that of TRPO, locating around 530 eV. The difference in the O K-edge XAS between TRPO and $UO_2Cl_2(TRPO)_2$ is supposed to be a result of two factors. One is that the only oxygen in TRPO is from the O═P moiety, whereas in the $UO_2Cl_2(TRPO)_2$ complexes, both the equatorial and axial oxygen atoms contribute to the pre-edge transitions. The other one is the covalent interaction between the uranyl ion and TRPO, which has been confirmed by the peak shift and intensity variation in comparing the P K-edge XAS for TRPO and $UO_2Cl_2(TRPO)_2$ in Figure 2.

The O K-edge XAS spectra of both TRPO and $UO_2Cl_2(TRPO)_2$ were modeled with Gaussian functions and a step function using an error function to identify the exact energy of the pre-edge features as well as to quantify the intensities. The energy positions of the peaks are determined by the second derivatives and are fixed during the curve fits (Figures S2 and S4). Other fitting parameters, including the peak amplitude and the half width, are entirely unconstrained. Figure 5 shows the modeling results for the pre-edge regions of the spectra for TRPO and $UO_2Cl_2(TRPO)_2$, and the complete fits and fitting parameters are provided in Figures S3 and S5 and Tables S5 and S6).

In the TRPO series, the best fits of the spectra for TPPO, CDPPO, and EDPPO are acquired using four pre-edge features from 531 to 537 eV. In contrast, using only three pre-edge features at 533.0, 534.0, and 535.1 eV can give a high-quality curve fit of the spectrum for TCyPO. For the $UO_2Cl_2(TRPO)_2$ complexes, all the spectra are adequately modeled by five resolved pre-edge features. Table 1 summarizes the transition energies and intensities in modeling the O K-edge XAS for $UO_2Cl_2(TRPO)_2$. All the spectra of $UO_2Cl_2(TRPO)_2$ reveal similar transition energies and intensities in the pre-edge regions, containing a low-intensity pre-edge shoulder at 529.8 eV, an intermediate-intensity pre-edge feature around 533.1 eV, and three high-intensity pre-edge features near 531.4, 534.6, and 536.0 eV.

Ground-State Electronic Structure of TRPO. The electronic structure of TRPO is investigated to clarify its orbitals that can interact with the uranyl ion and to provide a basis for interpreting the above O K-edge XAS of TRPO. In the O═P moiety of TRPO, the O 2p orbitals can mix with P 3p orbitals to form both σ- and π-bonds, as shown in Scheme 2, and the fragment orbitals of P═O can mix with the symmetry-adapted linear combinations (SALCs) of the orbitals from the three R substituents. Taking C_3-symmetric TPPO as an example, the three phenyl substitutions of TPPO provide

https://doi.org/10.1021/acs.inorgchem.1c02236
Inorg. Chem. XXXX, XXX, XXX−XXX

Table 1. Energy and Intensity Obtained by Curve-Fitting of the O K-edge XAS for $UO_2Cl_2(TRPO)_2$

transition	curve fitting: energy (eV)	curve fitting: intensity
$UO_2Cl_2(TPPO)_2$		
$1s \rightarrow 1b_{1u} + 1b_{2u} + 1b_{3u}$	529.8	0.12
$1s \rightarrow 2b_{2u} + 2b_{3u}$	531.4	1.41
$1s \rightarrow 1b_{1g}$	533.0	1.36
$1s \rightarrow 2b_{1u}$	534.6	2.10
$1s \rightarrow 1b_{2g} + 1b_{3g}$	536.0	2.58
$UO_2Cl_2(CDPPO)_2$		
$1s \rightarrow 1b_{1u} + 1b_{2u} + 1b_{3u}$	529.8	0.14
$1s \rightarrow 2b_{2u} + 2b_{3u}$	531.5	1.43
$1s \rightarrow 1b_{1g}$	533.4	1.42
$1s \rightarrow 2b_{1u}$	534.6	1.95
$1s \rightarrow 1b_{2g} + 1b_{3g}$	536.3	3.04
$UO_2Cl_2(EDPPO)_2$		
$1s \rightarrow 1b_{1u} + 1b_{2u} + 1b_{3u}$	529.8	0.14
$1s \rightarrow 2b_{2u} + 2b_{3u}$	531.4	1.83
$1s \rightarrow 1b_{1g}$	533.1	1.19
$1s \rightarrow 2b_{1u}$	534.6	3.19
$1s \rightarrow 1b_{2g} + 1b_{3g}$	536.4	3.59
$UO_2Cl_2(TCyPO)_2$		
$1s \rightarrow 1b_{1u} + 1b_{2u} + 1b_{3u}$	529.8	0.13
$1s \rightarrow 2b_{2u} + 2b_{3u}$	531.5	1.31
$1s \rightarrow 1b_{1g}$	533.5	1.38
$1s \rightarrow 2b_{1u}$	534.5	1.82
$1s \rightarrow 1b_{2g} + 1b_{3g}$	535.7	2.11

Scheme 2. Qualitative MOs Correlation Diagram of TRPO in C_3 Point Group Symmetry

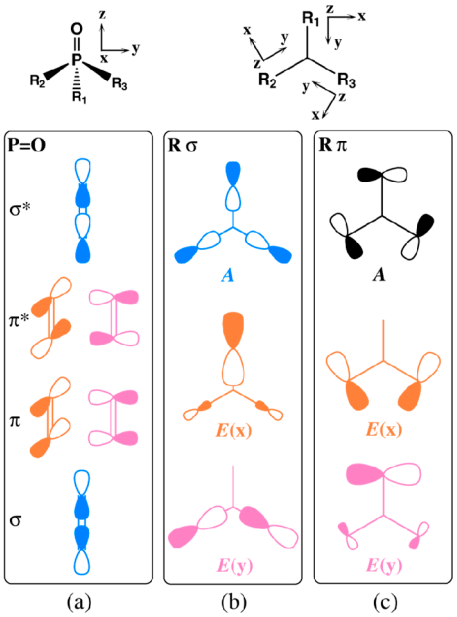

both σ- and π-type interactions with the O═P moiety. The σ-type SALCs of R orbitals span A and E symmetries to mix with the O═P σ- and π-type orbitals, respectively. The π-type SALCs of the R orbitals span A and E symmetries, whereas only those of E symmetry can mix with the O═P π-type orbitals. That of A symmetry cannot interact with the O═P σ- or π-type orbitals.

The bonding interactions within the TRPO molecules are confirmed by ground-state DFT calculations. Four canonical Kohn−Sham orbitals of TPPO calculated at the B3LYP/TZ2P level are illustrated in Figure 6. The truncated unoccupied

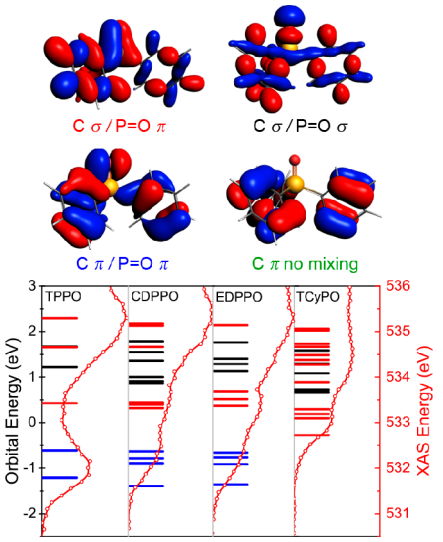

Figure 6. Contours of the representative MOs (0.03 au) for TPPO (top), and comparisons of the calculated MOs energy levels with the experimental O K-edge XAS for TRPO (bottom).

MOs energy level diagram for TRPO, which has been shifted by a constant to make the energies of O 1s orbitals equivalent to each other for comparison with the O K-edge XAS, is also presented in Figure 6. For the ligands TPPO, CDPPO, and EDPPO, there are orbitals belonging to the phenyl π-orbitals mixing with O═P π-orbitals between −1.5 and 0.5 eV. In contrast, TCyPO has no R π/P═O π-type MOs due to the lack of phenyl rings and therefore has no orbitals in this region. This difference is in perfect agreement with the experimental O K-edge XAS, where the transitions around 532 eV in the spectra for TPPO, CDPPO, and EDPPO are not observed in that for TCyPO. The remaining peaks at the region from 533 to 536 eV in the O K-edge XAS for all the TRPO complexes are attributed to the electronic transitions from O 1s orbitals to the unoccupied MOs formed by the mixing of R σ-orbitals with O═P (π + σ)-orbitals.

The group theory analysis and DFT calculations reveal that the TRPO ligands can provide both σ- and π-orbitals to interact with the uranyl ion in the $UO_2Cl_2(TRPO)_2$ complexes since oxygen in the O═P group can be both a σ- and π-donor. The hybridization of the O═P fragment orbitals depends on the type of the substituents in TRPO. The orbitals from phenyl rings can mix with the O═P fragment orbitals through both σ- and π-type bonding interactions, whereas the orbitals from alkyl substituents can only provide σ-orbitals to mix with the O═P fragment orbitals. Therefore, no transitions to R π/P═O π MOs are observed in the O K-edge XAS of TCyPO.

Ground-State Electronic Structure of $UO_2Cl_2(TRPO)_2$. The chemical bonding interactions between uranyl moiety and TRPO ligands in $UO_2Cl_2(TRPO)_2$ are analyzed by group theory and DFT calculations, and the discussion will focus on the unoccupied orbitals most relevant to the O K-edge XAS experiments. In the O K-edge XAS of $UO_2Cl_2(TRPO)_2$, both the O_{eq} and O_{yl} atoms contribute to the pre-edge transitions. The bonding interactions between U and O_{yl} have been widely

https://doi.org/10.1021/acs.inorgchem.1c02236
Inorg. Chem. XXXX, XXX, XXX−XXX

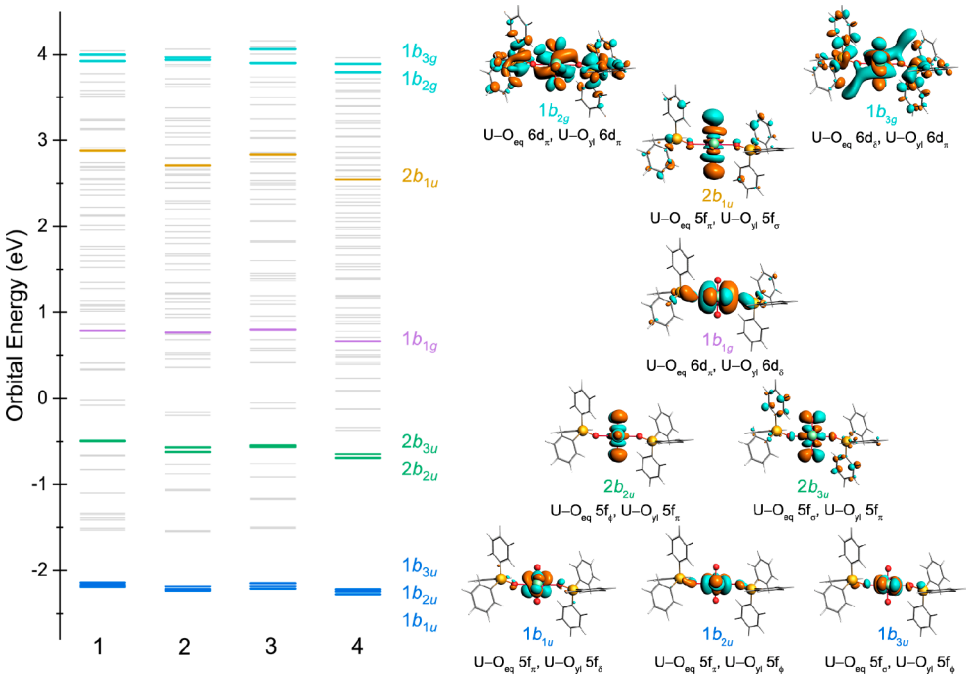

Figure 7. Truncated MOs energy levels for $UO_2Cl_2(TRPO)_2$ calculated at DFT/B3LYP level (left) and the contours of unoccupied Kohn−Sham orbitals (0.02 au) relevant to the orbital interactions between the uranyl ion and TRPO (right).

studied. The two axial U−O_{yl} triple bonds are formed by mixing of U 5f and 6d orbitals with the O_{yl} 2p orbitals, resulting in two σ- and four π-bonding orbitals ($\sigma_u^2\pi_u^4\sigma_g^2\pi_g^4$).[19−21,66] For the chemical bonding between the uranyl ion and the equatorial oxygen atoms from TRPO ligands, it is quite simplistic to perform group theory analysis on $UO_2Cl_2(TRPO)_2$ assuming D_{2h} symmetry by ignoring the phosphorus atom of TRPO and the substituents on it. The fragment orbitals provided by the two TRPO molecules can form four π-type SALCs spanning b_{1u} + b_{2u} + b_{1g} + b_{2g} symmetries and two σ-type SALCs spanning b_{3u} + a_g symmetries. The SALCs of b_{1u} and b_{2u} symmetries can mix with the U 5f orbitals to form π U−TRPO bonding interactions of $1b_{1u}$ (U−O_{eq} 5f_π, U−O_{yl} 5f_δ), $1b_{2u}$ (U−O_{eq} 5f_π, U−O_{yl} 5f_φ), and $2b_{1u}$ (U−O_{eq} 5f_π, U−O_{yl} 5f_σ) symmetries. The SALCs of b_{3u} symmetry can mix with the U 5f orbitals to form σ U−TRPO bonding interactions of $1b_{3u}$ (U−O_{eq} 5f_σ, U−O_{yl} 5f_φ) and $2b_{3u}$ (U−O_{eq} 5f_σ, U−O_{yl} 5f_π) symmetries. This leaves the U 5f orbital of $1a_u$ (U−O_{eq} 5f_δ, U−O_{yl} 5f_δ) symmetry as nonbonding with respect to both O_{eq} and O_{yl} atoms and that of $2b_{2u}$ (U−O_{eq} 5f_φ, U−O_{yl} 5f_π) symmetry as nonbonding with respect to O_{eq} atoms and π-bonding with respect to O_{yl} atoms. For the chemical bonding between TRPO and U 6d orbitals, the SALCs of b_{1g} + b_{2g} symmetries can mix with the U 6d orbitals to form π U−TRPO bonding interactions of $1b_{1g}$ (U−O_{eq} 6d_π, U−O_{yl} 6d_δ) and $1b_{2g}$ (U−O_{eq} 6d_π, U−O_{yl} 6d_π) symmetries. The SALCs of a_g symmetries can mix with the U 6d orbitals to form σ U−TRPO bonding interactions of $1a_g$ (U−O_{eq} 6d_σ, U−O_{yl} 6d_δ) and $2a_g$ (U−O_{eq} 6d_σ, U−O_{yl} 6d_σ) symmetries. This leaves the U 6d orbital of b_{3g} (U−O_{eq} 6d_δ, U−O_{yl} 6d_π) symmetry as nonbonding with respect to O_{eq} atoms and π-bonding with respect to O_{yl} atoms. Figure 7 shows the truncated energy levels of the unoccupied MOs of $UO_2Cl_2(TRPO)_2$ obtained from ground-state DFT calculations. Orbitals of σ-type ($1b_{3u}$ and $2b_{3u}$) and π-type ($1b_{1u}$, $1b_{2u}$ and $2b_{1u}$) interactions between O_{eq} 2p and U 5f orbitals and orbitals of π-type ($1b_{1g}$ and $1b_{2g}$) interactions between O_{eq} 2p and U 6d orbitals can be observed in DFT calculations. Orbitals of σ-type bonding interactions between O_{eq} 2p and U 6d orbitals in a_g symmetry are not observable because their energies are too high, resembling the case of $UO_2Cl_4^{2-}$.[37] The energies of the MOs associated with the bonding interactions between the uranyl ion and TRPO are very similar for the four $UO_2Cl_2(TRPO)_2$ complexes, and this is consistent with the XAS spectra where the substituents have little effect on the pre-edge energies. It is worth mentioning that some orbitals with energies above −1.5 eV contain O 2p components but no U 5f or 6d orbitals. These orbitals also contribute slightly to the pre-edge transitions in the O K-edge XAS, as suggested by TDDFT calculations (*vide infra*).

According to the orbital energies provided by the ground-state DFT calculations in Figure 7, the five pre-edge features (from left to right) around 529.8, 531.4, 533.2, 534.6, and 536.0 eV, obtained by curve-fitting analysis in the O K-edge XAS of the $UO_2Cl_2(TRPO)_2$ complexes in Figure 5, are reasonably assigned to the transitions from O 1s orbitals to the unoccupied MOs of $1b_{1u}$ + $1b_{2u}$ + $1b_{3u}$, $2b_{2u}$ + $2b_{3u}$, $1b_{1g}$, $2b_{1u}$, and $1b_{2g}$ + $1b_{3g}$ symmetries, respectively. The transitions from O 1s orbitals to the unoccupied MOs of $1b_{1u}$ + $1b_{2u}$ + $1b_{3u}$ and $1b_{1g}$ symmetries are contributed by the oxygen atoms of TRPO. The other three transitions to the orbitals of $2b_{2u}$ + $2b_{3u}$, $2b_{1u}$, and $1b_{2g}$ + $1b_{3g}$ symmetries are contributed by both the equatorial and axial oxygen atoms. The O_{yl} K-edge XAS for the uranyl complexes where no oxygen atoms are present in the equatorial plane have been examined previously.[20,21,67] For example, Denning et al. examined the O_{yl} K-edge XAS for $Cs_2UO_2Cl_4$ and found three pre-edge features at 531.4, 534.1, and 536.5 eV, corresponding to the transitions from O_{yl} 1s orbitals to the unoccupied orbitals of U−O_{yl} 5f_π, U−O_{yl} 5f_σ, and U−O_{yl} 6d_π, respectively.[20,21] These values match well with our findings for $UO_2Cl_2(TRPO)_2$ at 531.4 eV, 534.6, and 536.0 eV.

https://doi.org/10.1021/acs.inorgchem.1c02236
Inorg. Chem. XXXX, XXX, XXX−XXX

Hybrid TDDFT Spectral Simulations. The TDDFT calculations on TRPO and $UO_2Cl_2(TRPO)_2$ are carried out to obtain the simulated spectra for direct comparison with the experiment XAS, and the results are shown in Figure 8. The

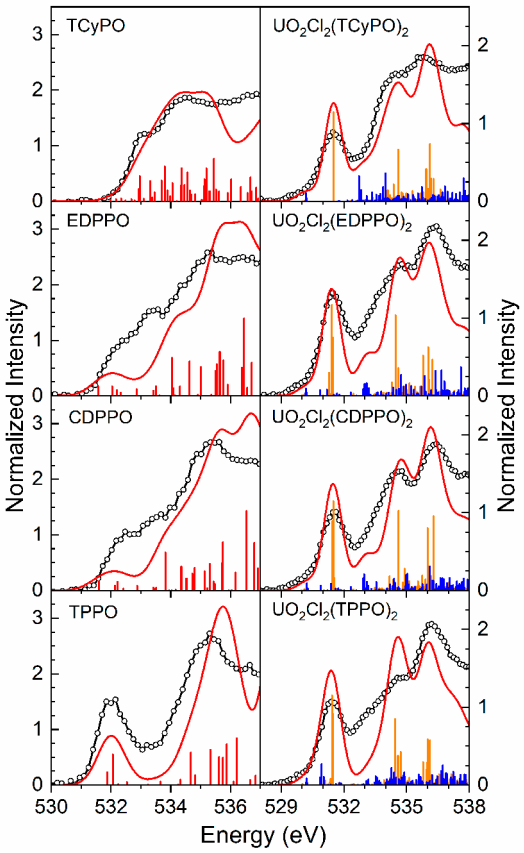

Figure 8. Comparison of the simulated spectra obtained by TDDFT calculations (red) with the experimental O K-edge XAS data for TRPO and $UO_2Cl_2(TRPO)_2$ (black). The bars represent the energies and oscillator strengths for the individual transitions. The blue and orange bars represent the transitions from O_{eq} and O_{yl} 1s orbitals, respectively, in the TDDFT calculations for $UO_2Cl_2(TRPO)_2$.

simulated spectra have been shifted by approximately +14.3 eV for TRPO and +12.4 eV for $UO_2Cl_2(TRPO)_2$ to account for the omission of the atomic and extra-atomic relaxation associated with the core excitation, relativistic stabilization, and errors associated with the functional.[68,69]

The simulated spectra of TRPO match well with the experimental data, with a slight discrepancy in relative intensity. The transitions around 532 eV in the simulated spectra for TPPO, CDPPO, and EDPPO are not observed for TCyPO, consistent with the experimental spectra. The TDDFT simulations confirm that the pre-edge regions from 533 to 536 eV in the O K-edge XAS spectra for TRPO are attributed to the electronic transitions from O 1s orbitals to the unoccupied MOs formed by the mixing of R σ-orbitals with P═O ($\sigma + \pi$)-orbitals.

For the spectra of $UO_2Cl_2(TRPO)_2$, the electronic transitions from O_{eq} and O_{yl} 1s orbitals to the unoccupied MOs were calculated separately, and the transitions are depicted by blue and orange bars, respectively, in Figure 8. One can see that five transition features in TDDFT simulated spectra are resolved, matching well with the experimental data. Although there is no way to experimentally discriminate the contributions from O_{eq} and O_{yl} atoms to the XAS spectra of $UO_2Cl_2(TRPO)_2$, TDDFT calculations confirm the assignments of transitions in DFT calculations that the first feature at 529.8 eV in each spectrum is entirely attributed to the transitions from O_{eq} 1s orbitals to the unoccupied MOs of $1b_{1u} + 1b_{2u} + 1b_{3u}$ symmetries, which are associated with the covalent mixing between O_{eq} 2p orbitals and U 5f orbitals. The transitions from O_{eq} and O_{yl} 1s orbitals to unoccupied MOs both contribute to the pre-edge features at 531.4, 534.6, and 536.0 eV obtained by curve fits in Figure 5, with O_{yl} contributing much more than O_{eq}. The pre-edge feature around 533.2 eV is contributed by the transition from O_{eq} 1s orbitals to the orbital of $1b_{1g}$ symmetry, and there are no transitions from O_{yl} 1s orbitals to the unoccupied orbitals. As mentioned above, some orbitals containing O 2p components that do not mix with U 5f or 6d orbitals can contribute slightly to the pre-edge transitions from O 1s orbitals to the orbitals of $1b_{1g}$ symmetry as well as to those of $2b_{2u} + 2b_{3u}$, $2b_{1u}$, and $1b_{2g} + 1b_{3g}$ symmetries. In such a context, only the transitions from O 1s orbitals to the orbitals of $1b_{1u} + 1b_{2u} + 1b_{3u}$ symmetries exclusively reflect the U−O_{eq} covalent bonding interactions.

Evaluation of the Bonding Covalency between the Uranyl Ion and TRPO. The intensity of the pre-edge feature observed in ligand K-edge XAS spectra correlates to the degree of ligand *n*p orbital mixing in metal-derived MOs according to the relationship[29,70]

$$I = \frac{1}{N} h\alpha^2 I_0 \quad (1)$$

where I is the integrated pre-edge area for the normalized spectrum, N is the number of absorbing ligand atoms, h is the number of electron holes, α^2 is the p character per electron−hole in the acceptor molecular orbital, and I_0 is the intrinsic transition dipole integral for ligand 1s → *n*p excitations that is dependent on the property of the sample, sample preparation, detection method, and beamline end-station and upstream optics. To obtain α^2 from the pre-edge intensity requires the value of the intrinsic transition dipole integral I_0. In the quantitative study of lanthanide-oxygen orbital mixing in CeO_2, PrO_2, and TbO_2, Minasian et al. compared the pre-edge intensities associated with Ln 4f orbitals in the O K-edge XAS spectra to the relative intensities of the two peaks in the Ln L_3-edge XAS and estimated a value of 9.86 for the intrinsic intensity of O 1s → 2p transition.[46] This value is comparable to 10.3 for the photoabsorption cross-section of atomic oxygen reported by McLaughlin et al.[71] As mentioned above, many factors affect the intrinsic intensity of I_0, such as the sample properties and detection method. In this work, the method to collect the XAS spectra is TFY, in which the intrinsic intensity is proportional to the X-ray absorption cross section. Saturation and self absorption effects must be considered because they can cause fluorescence yield variations, resulting in the variation of the pre-edge transition intensities.[72,73] Besides, the effective charge dependence of the transition dipole moment integral should be taken into account, as reported by Neese et al.[74] In this context, it is not appropriate to directly convert the experimental pre-edge intensity of the O K-edge XAS in Figure 5 to percent O 2p character using the value of the intrinsic intensity obtained from lanthanide dioxides or atomic oxygen. In this work, therefore, we use the data from Mulliken population analysis that are intimately

https://doi.org/10.1021/acs.inorgchem.1c02236
Inorg. Chem. XXXX, XXX, XXX−XXX

associated with the experimental XAS data to evaluate the bonding covalency between the uranyl ion and TRPO ligands.

Table 2 summarizes the DFT calculated percent O_{eq} and O_{yl} 2p character for the MOs showing in Figure 7 that are relevant to the pre-edge transitions in the O K-edge XAS of the $UO_2Cl_2(TRPO)_2$ complexes. Taking $UO_2Cl_2(TPPO)_2$ as an example, the amount of O_{eq} 2p character in the π-bonding with U 5f orbitals of $1b_{1u}$, $1b_{2u}$, and $2b_{1u}$ symmetries are 0.39, 1.00, and 0.37, respectively, and that in the σ-bonding with U 5f orbitals of $1b_{3u}$ and $2b_{3u}$ symmetries are 0.35 and 0.16, respectively. The amount of O_{eq} 2p character in the π-bonding with U 6d orbitals of $1b_{1g}$ and $1b_{2g}$ symmetries are 1.00 and 0.26, respectively. All the amounts of O_{eq} 2p character are very small and much lower than that of O_{yl} 2p character. For example, the amount of O_{yl} 2p character in π-bonding with U 5f orbitals of $2b_{2u}$ and $2b_{3u}$ symmetries are 21.19 and 18.97, respectively. Upon the variation of the TRPO ligands in the $UO_2Cl_2(TRPO)_2$ complexes, the amounts of O_{eq} 2p character are very similar, indicating the insignificant effect of the substituents in TRPO on the bonding interaction with the uranyl ion.

Table 2. Mulliken Population Analysis for the $UO_2Cl_2(TRPO)_2$ Complexes

MO[a]	energy (eV)	Mulliken population (DFT, %) O_{eq} 2p	O_{yl} 2p	Cl 3p
		$UO_2Cl_2(TPPO)_2$		
$1b_{1u}$	−2.19	0.39		2.51
$1b_{2u}$	−2.17	1.00		4.37
$1b_{3u}$	−2.15	0.35		3.67
$2b_{2u}$	−0.50		21.19	2.43
$2b_{3u}$	−0.49	0.16	18.97	
$1b_{1g}$	0.79	1.00		5.60
$2b_{1u}$	2.88	0.37	37.31	0.26
$1b_{2g}$	3.93	0.26	8.93	
$1b_{3g}$	4.00		9.24	2.64
		$UO_2Cl_2(CDPPO)_2$		
$1b_{1u}$	−2.31	0.64		2.35
$1b_{2u}$	−2.29	1.10		4.63
$1b_{3u}$	−2.26	0.20		3.68
$2b_{2u}$	−0.64		20.85	2.50
$2b_{3u}$	−0.69	0.01	18.99	
$1b_{1g}$	0.70	1.15		5.02
$2b_{1u}$	2.64	0.37	15.24	0.03
$1b_{2g}$	3.87	0.23	7.65	
$1b_{3g}$	3.90		7.83	0.66
		$UO_2Cl_2(EDPPO)_2$		
$1b_{1u}$	−2.30	0.41		2.61
$1b_{2u}$	−2.26	1.13		4.62
$1b_{3u}$	−2.23	0.52		3.74
$2b_{2u}$	−0.64		20.92	2.54
$2b_{3u}$	−0.63	0.19	18.80	
$1b_{1g}$	0.72	1.31		5.39
$2b_{1u}$	2.75	0.39	19.52	0.29
$1b_{2g}$	3.82	0.26	10.01	
$1b_{3g}$	3.98		9.03	1.32
		$UO_2Cl_2(TCyPO)_2$		
$1b_{1u}$	−2.14	0.65		2.32
$1b_{2u}$	−2.11	1.28		4.58
$1b_{3u}$	−2.08	0.42		3.66
$2b_{2u}$	−0.55		20.69	2.56
$2b_{3u}$	−0.51	0.01	18.92	
$1b_{1g}$	0.80	0.50		4.41
$2b_{1u}$	2.68	0.16	10.07	0.06
$1b_{2g}$	3.93	0.68	5.51	
$1b_{3g}$	4.03		6.31	2.75

[a]Orbitals at high energy levels, e.g., $2b_{1u}$, $1b_{2g}$, and $1b_{3g}$, split into two or more orbitals, among which the highest orbital composition is presented in the table.

As mentioned above, only the pre-edge feature around 529.8 eV in each spectrum is exclusively attributed to the transitions from O_{eq} 1s orbitals to the unoccupied MOs of $1b_{1u} + 1b_{2u} + 1b_{3u}$ symmetries. The total amount of O_{eq} 2p character of the orbitals of $1b_{1u} + 1b_{2u} + 1b_{3u}$ symmetries in Mulliken population are 1.74, 1.94, 2.06, and 2.37% in $UO_2Cl_2(TPPO)_2$, $UO_2Cl_2(CDPPO)_2$, $UO_2Cl_2(EDPPO)_2$, and $UO_2Cl_2(TCyPO)_2$, respectively. These small values are consistent with the small intensity of the first pre-edge feature in the O K-edge XAS spectra for the $UO_2Cl_2(TRPO)_2$ complexes. In contrast, the total amount of O_{yl} 2p character in the orbitals of $2b_{2u} + 2b_{3u}$ symmetries in Mulliken population are remarkably large, corresponding to the high intensity of the pre-edge features around 531.4 eV in the O K-edge XAS of the $UO_2Cl_2(TRPO)_2$ complexes. In general, both the experimental O K-edge XAS results and DFT calculations clearly indicate a very small amount of covalent bonding between the uranyl ions and TRPO ligands in the $UO_2Cl_2(TRPO)_2$ complexes.

Although there have been many studies on the interactions between the uranyl ion and ligands on its equatorial plane, few have evaluated the bonding covalency. Spencer et al. examined the Cl K-edge XAS for $[Ph_4P]_2[UO_2Cl_4]$ and found that the total amount of percent Cl 3p character observed with the U 5f orbitals was roughly 7.6% per U−Cl bond.[37] According to the intensities of the pre-edge features obtained by curve-fitting analysis on the Cl K-edge XAS for the $UO_2Cl_2(TRPO)_2$ complexes (Figure S6 and Tables S7 and S8), the amount of percent Cl 3p character with the U 5f orbitals is from 6.53 to 8.02 per U−Cl bond in the $UO_2Cl_2(TRPO)_2$ complexes. DFT calculations (Table 2) reveal that the total amount of Cl 3p character in the orbitals of $1b_{1u} + 1b_{2u} + 1b_{3u} + 2b_{2u}$ symmetries are 12.98, 13.16, 13.51, and 13.12, corresponding to 6.49, 6.58, 6.76, and 6.56 per U−Cl bond in $UO_2Cl_2(TPPO)_2$, $UO_2Cl_2(CDPPO)_2$, $UO_2Cl_2(EDPPO)_2$, and $UO_2Cl_2(TCyPO)_2$, respectively. The XAS experiments and DFT calculations agree very well with each other. The Mulliken population analysis suggests that the U 5f orbitals participate more in mixing with Cl 3p orbitals than in mixing with O_{eq} 2p orbitals in the $UO_2Cl_2(TRPO)_2$ complexes. Furthermore, both the experimental and theoretical results quantitatively confirm the conclusion aforementioned that the interactions of Cl 3p orbitals with the U 5f and 6d orbitals are not significantly perturbed when varying the other equatorial ligands in the uranyl complexes.

CONCLUSION AND OUTLOOK

We have detected for the first time the covalency of the U(VI)−TRPO system that is actually used in separation processes using the technique of oxygen K-edge X-ray absorption spectroscopy (XAS) in combination with density functional theory (DFT) calculations. The primary purpose of this work is to investigate the contributions of U 6d and especially 5f orbitals to the bonding covalency between the uranyl ion and TRPO on its equatorial plane in order to

https://doi.org/10.1021/acs.inorgchem.1c02236
Inorg. Chem. XXXX, XXX, XXX−XXX

elucidate the extrodinary extractability and selectivity of the monodentate organophosphorus extractants to the uranyl ion. Using the O K-edge XAS technique and DFT calculations, we have detected the electronic structure of both the free ligands TRPO and the complexes $UO_2Cl_2(TRPO)_2$. Although the TRPO ligands display substantially different pre-edge features depending on whether their substituents can provide π-orbitals to mix with the O=P orbitals, all the TRPO investigated can engage in σ- and π-type interactions with U 5f and 6d orbitals in the $UO_2Cl_2(TRPO)_2$ complexes. All the $UO_2Cl_2(TRPO)_2$ complexes show similar pre-edge features in O K-edge XAS, indicating that substituents on TRPO have little effect on the covalent bonding between TRPO and UO_2^{2+}. The first pre-edge feature in the O K-edge XAS of $UO_2Cl_2(TRPO)_2$ is identified as the transitions to the U 5f orbitals of $1b_{1u} + 1b_{2u} + 1b_{3u}$ symmetries, which are exclusively contributed by the σ- and π-type mixing between U 5f and O_{eq} 2p orbitals. Curve-fitting analysis indicates small intensities of 0.12−0.14 for this pre-edge feature of the $UO_2Cl_2(TRPO)_2$ complexes, which are consistent with the small amount of O_{eq} 2p character (1.74−2.37%) as obtained by Mulliken population analysis. Other pre-edge features in the O K-edge XAS of $UO_2Cl_2(TRPO)_2$ are dominantly contributed by the U−O_{yl} orbital mixing, and the contributions of the U−O_{eq} orbital mixing cannot be extracted from the experimental spectra. Nonetheless, DFT calculations reveal that both U 5f and 6d orbitals can participate in U−TRPO σ- and π-type covalent bonding interactions.

To thoroughly reveal the role of covalency in extraction separation, additional work is warranted in the future, as there are many factors that can affect the extraction efficiency, such as the geometries of the extracted species and the aggregation behavior in the organic phase. Nevertheless, we believe that the covalent bonding interactions between TRPO and UO_2^{2+}, especially the contributions from U 5f orbitals, play the central role in achieving the remarkable extractability and selectivity of TRPO for the uranyl ion. Cross et al. reported that the amount of Cl 3p character mixing with Am 5f orbitals is 0.54(5)% per Am−Cl bond for $AmCl_6^{3-}$. In contrast, for $EuCl_6^{3-}$ the amount of Cl 3p orbital mixing in the Eu−Cl bond is too small to quantify and significantly less than the 0.54(5)% value for $AmCl_6^{3-}$. The subtle differences between Am 5f orbitals in Am−Cl orbital mixing and Eu 4f orbitals in Eu−Cl orbital mixing are considered to have the potential to achieve the appreciable Am/Eu separations,[38] because only ∼0.4 kcal/mol/bond is needed to achieve appreciable Am/Eu separations.[75] In the present work, the total amount of mixing between U 5f and O_{eq} 2p orbitals is 0.87−1.18% per U−O_{eq} bond as obtained by Mulliken population analysis. This value is relatively small, but it is supposed to be sufficiently significant for achieving a high distribution ratio in an extraction, according to the work by Cross and co-workers.[38] In contrast, it is not necessarily the case that more covalency would induce stronger interactions between metal ions and ligands. Covalent interactions between the ligands and metal ions are usually accompanied by ligand-to-metal charge transfer interactions, which would act to weaken the stabilization of the metal−ligand complexes due to the reduced ionic attraction by decreasing the charge differential.[76] Therefore, too much covalency between the ligands and metal ions can be counterproductive to extraction and separation. This is reminiscent of the multidentate ligands with both hard and soft donor atoms that possess high extractability and selectivity toward actinides. The soft donor atoms play the role to covalently interact with the metal ions to enhance the selectivity in extraction, while the hard donor atoms retain the affinity and thus the remarkable extractability toward the metal ions.[77−81] Accordingly, the TRPO ligands can serve the combined soft−hard strategy in the extraction of uranyl ions, in which a small amount of covalency based on the strong affinity achieve the remarkable selectivity and extractability of TRPO toward the uranyl ions.

EXPERIMENTAL SECTION

Sample Preparation. ***Caution!*** *Standard precautions for handling radioactive materials should be implemented due to the slightly radioactive uranium used in this work.*

Single crystals of TRPO suitable for X-ray diffraction characterization were obtained by recrystallization from dichloromethane/*n*-heptane in a glovebox, according to the procedure reported in the literature.[56] Single crystals of the uranyl complexes $UO_2Cl_2(TRPO)_2$ were prepared using the reported procedures with slight modifications.[13] Detailed procedures for the synthesis of $UO_2Cl_2(TRPO)_2$ are illustrated in the Supporting Information. $[PPh_4]_2[UO_2Cl_4]$ was synthesized and crystallized from the reaction of hydrated uranyl nitrate with tetraphenylphosphonium chloride in acetonitrile followed by slow evaporation in atmosphere condition based on the reports in the literature with some modification.[82,83]

X-ray Crystallography. The single-crystal X-ray diffraction data were collected on a Super Nova, Dual, Cu at zero, AtlasS2 (Rigaku) using Cu Kα (λ = 1.54184 Å) or Mo Kα (λ = 0.71073 Å) radiation. All crystals were measured at low temperature (104−173 K). Data collection and reduction were carried out in CrysAlisPro 1.171.39.46 (Rigaku Oxford Diffraction, 2018). The structure solution and refinement were carried out with SHLEX-97 and Olex2 1.2 program.[84,85] The absorption data were corrected using the multiscan method. The structure was solved by direct methods or Intrinsic Phasing method and was refined against F^2 by full-matrix least-squares techniques. All non-hydrogen atoms were refined with anisotropic displacement parameters. The hydrogen atoms were added according to the ideal geometry and were not refined for good refinement convergence. Data collection and refinement details are available in Tables S1 and S2. The crystallographic information files (CIFs) mentioned this manuscript are available through the Cambridge Crystal Data Centre (CCDC 2043630−2043637).

XAS Measurements and Data Analysis. The O K-edge XAS data were recorded at beamline 02B02 of Shanghai Synchrotron Radiation Facility (SSRF) running in electron storage ring mode at 3.5 GeV and with current at 240 mA.[86] The energy range of the beamline 02B02 is from 40 to 2000 eV. The measured photon flux is around 10^{11} photons/s with $E/\Delta E$ = 3700 at 244 eV. The beam spot size at a sample is measured to be about 150 μm × 50 μm. Grating was optimized with line densities of 400 lines mm^{-1} covering the energy ranges 40−600 eV to obtain high-energy resolution. The XAS data were collected by total fluorescence yield (TFY) mode in an ultrahigh vacuum chamber about 5 × 10^{-9} Torr. The energy steps of 1, 0.15, 0.3, 1, and 2 eV were used between 500 and 530, 530−545, 545−560, 560−580, and 580−600 eV, respectively, to collect the O K-edge XAS data. The P and Cl K-edge XAS data were recorded at beamline 4B7A of Beijing Synchrotron Radiation Facility (BSRF) over an energy range from 1750 to 6000 eV in partial fluorescence yield (PFY) mode using a 13-element Si (Li) array detector.[87] The energy of the electron beam is 2.5 GeV in the storage ring, where the maximum beam current is 250 mA. The beam spot size at a sample is about 1.5 mm × 0.4 mm, and the measured flux is over 3 × 10^{10} photons/s/250 mA.

Single-crystal samples were ground into a fine powder and dispersed on carbon tape for P and Cl K-edge XAS measurements and indium films for O K-edge XAS measurements. The energy scales in the O, P, and Cl K-edge XAS were calibrated using $SrTiO_3$, $Na_4P_2O_7$, and D_{2d}-Cs_2CuCl_4 standard, respectively, which were

https://doi.org/10.1021/acs.inorgchem.1c02236
Inorg. Chem. XXXX, XXX, XXX−XXX

repeatedly analyzed between sample scans. All the spectra were collected in duplicate at least twice. Spectra showed no signs of radiation damage and were reproduced over multiple regions of the sample.

The background subtraction and normalization of O, P, and Cl K-edge XAS data were manipulated using the Athena interface in the Demeter software program.[88] In a typical example, a line was fit to the pre-edge region and then subtracted from the experimental data to eliminate the background of the spectrum. The data were normalized to a unit step height by fitting a second-order polynomial to the postedge region of the spectrum. Curve-fitting of the O K-edge XAS was carried out using the program IGOR pro 8.04 and a modified version of EDG_FIT.[89] Second derivative spectra were used as guides to determine the number and position of peaks (Figures S1 and S3). Pre-edge and rising edge features were modeled by Gaussian line shapes and an error function, respectively (Figures S2 and S4). Fits were carried out over several energy ranges. The quality of each curve fit was determined by evaluating changes in the χ^2 and by inspecting the residual intensity, which is obtained by subtracting the fit from the experiment data and should resemble a horizontal line at zero. The area under the pre-edge peaks (defined as the intensity) was used as the transition intensity.

DFT and TDDFT Calculation. All DFT computations were carried out with the Amsterdam Density Functional (ADF 2019) program,[90,91] using the B3LYP hybrid functional.[92,93] The all-electron Slater type orbital (STO) basis sets of triple-ζ augmented by two sets of polarization functions (TZ2P) were employed to describe all atoms. Zero-order regular approximation (ZORA) was used to consider the scalar relativistic (SR) effects.[94] The geometries were optimized for TRPO and $UO_2Cl_2(TRPO)_2$, and the selected average bond lengths and bond angles were comparable to the values in the experimental crystals (Tables S3 and S4). To obtain the values of Mulliken populations larger than 0.01%, the keyword "ORBPOP" was used in single-point calculations.

The O K-edge XAS spectra for all complexes were simulated using of simplified TDDFT (sTDDFT) method.[95,96] For the TDDFT calculations at the ground-state optimized geometry, only excitations from O 1s core levels to virtual orbitals were analyzed by restricting the energy range of core level and virtual orbitals involved in excitation. The calculated oscillator strengths were evenly broadened with a Gaussian function of full-width at half maximum of 1 eV to generate the simulated absorption spectra. An energy shift was applied by aligning the experimental and calculated pre-edge peaks to account for the omission of the atomic and extra-atomic relaxation associated with the core excitation, relativistic stabilization, and errors associated with the functional, according to the literature.[68,69]

■ ASSOCIATED CONTENT

Supporting Information

The Supporting Information is available free of charge at https://pubs.acs.org/doi/10.1021/acs.inorgchem.1c02236.

Experiments and results for the solvent extraction of the uranyl ion by the ligands used in the present work, detailed procedure for the crystallization of the $UO_2Cl_2(TRPO)_2$ complexes, crystallographic data, bond lengths and bond angles for the TRPO and $UO_2Cl_2(TRPO)_2$ complexes, complete curve-fitting of the XAS spectra, and the analysis of the Cl K-edge XAS for the $UO_2Cl_2(TRPO)_2$ complexes (PDF)

Accession Codes

CCDC 2043630−2043637 contain the supplementary crystallographic data for this paper. These data can be obtained free of charge via www.ccdc.cam.ac.uk/data_request/cif, or by emailing data_request@ccdc.cam.ac.uk, or by contacting The Cambridge Crystallographic Data Centre, 12 Union Road, Cambridge CB2 1EZ, UK; fax: +44 1223 336033.

■ AUTHOR INFORMATION

Corresponding Author

Taoxiang Sun − *Institute of Nuclear and New Energy Technology, Tsinghua University, Beijing 100084, China;* orcid.org/0000-0003-4690-3566; Email: sunstx@tsinghua.edu.cn

Authors

Yusheng Zhang − *Institute of Nuclear and New Energy Technology, Tsinghua University, Beijing 100084, China*

Wuhua Duan − *Institute of Nuclear and New Energy Technology, Tsinghua University, Beijing 100084, China*

Yuning Yang − *Institute of Nuclear and New Energy Technology, Tsinghua University, Beijing 100084, China*

Tian Jian − *Chemical Sciences Division, Lawrence Berkeley National Laboratory, Berkeley, California 94720, United States;* orcid.org/0000-0002-2448-4666

Yusen Qiao − *Chemical Sciences Division, Lawrence Berkeley National Laboratory, Berkeley, California 94720, United States;* orcid.org/0000-0001-7654-8636

Guoxi Ren − *Shanghai Institute of Microsystem and Information Technology, Chinese Academy of Sciences, Shanghai 200050, China*

Nian Zhang − *Shanghai Institute of Microsystem and Information Technology, Chinese Academy of Sciences, Shanghai 200050, China;* orcid.org/0000-0002-9124-6553

Lei Zheng − *Institute of High Energy Physics, Chinese Academy of Sciences, Beijing 100049, China*

Wensheng Yan − *University of Science and Technology of China, National Synchrotron Radiation Laboratory, Hefei 230029, China;* orcid.org/0000-0001-6297-4589

Jianchen Wang − *Institute of Nuclear and New Energy Technology, Tsinghua University, Beijing 100084, China*

Jing Chen − *Institute of Nuclear and New Energy Technology, Tsinghua University, Beijing 100084, China*

Stefan G. Minasian − *Chemical Sciences Division, Lawrence Berkeley National Laboratory, Berkeley, California 94720, United States;* orcid.org/0000-0003-1346-7497

Complete contact information is available at: https://pubs.acs.org/10.1021/acs.inorgchem.1c02236

Notes

The authors declare no competing financial interest.

■ ACKNOWLEDGMENTS

This study is supported by the National Natural Science Foundation of China (21976103 and U1830202). S.G.M. was supported by the Director, Office of Science, Office of Basic Energy Sciences, Division of Chemical Sciences, Geosciences, and Biosciences (CSGB), Heavy Element Chemistry program of the U.S. Department of Energy (DOE) under contract no. DE-AC02-05CH11231 at LBNL. We are grateful to Ming Li (Tsinghua University) for his help with the single-crystal structures and Zhixian Wang (Peking University) for her help with the element analysis. The XAS data in this work were carried out with the support of 02B02 beamline of Shanghai Synchrotron Radiation Facility (SSRF), 4B7A beamline at Beijing Synchrotron Radiation Facility, and BL12B beamline of National Synchrotron Radiation Laboratory (NSRL) of China.

https://doi.org/10.1021/acs.inorgchem.1c02236
Inorg. Chem. XXXX, XXX, XXX−XXX

REFERENCES

(1) Mathur, J. N.; Murali, M. S.; Nash, K. L. Actinide partitioning - A review. *Solvent Extr. Ion Exch.* **2001**, *19* (3), 357−390.

(2) Beltrami, D.; Cote, G.; Mokhtari, H.; Courtaud, B.; Moyer, B. A.; Chagnes, A. Recovery of uranium from wet phosphoric acid by solvent extraction processes. *Chem. Rev.* **2014**, *114* (24), 12002−12023.

(3) Abney, C. W.; Mayes, R. T.; Saito, T.; Dai, S. Materials for the recovery of uranium from seawater. *Chem. Rev.* **2017**, *117* (23), 13935−14013.

(4) Keener, M.; Hunt, C.; Carroll, T. G.; Kampel, V.; Dobrovetsky, R.; Hayton, T. W.; Menard, G. Redox-switchable carboranes for uranium capture and release. *Nature* **2020**, *577* (7792), 652−655.

(5) Leoncini, A.; Huskens, J.; Verboom, W. Ligands for f element extraction used in the nuclear fuel cycle. *Chem. Soc. Rev.* **2017**, *46*, 7229−7273.

(6) Chen, J.; He, X. H.; Wang, J. C. Nuclear fuel cycle-oriented actinides separation in China. *Radiochim. Acta* **2014**, *102* (1−2), 41−51.

(7) Bombieri, G.; Forsellini, E.; Day, J. P.; Azeez, W. I. Crystal and molecular-structure of "dichlorodioxobis(triphenylphosphine oxide)-uranium(VI). *J. Chem. Soc., Dalton Trans.* **1978**, *6*, 677−680.

(8) Akona, S. B.; Fawcett, J.; Holloway, J. H.; Russell, D. R.; Leban, I. Structures of cis and trans-dichlorodioxobis(triphenylphosphine oxide)-uranium(VI). *Acta Crystallogr., Sect. C: Cryst. Struct. Commun.* **1991**, *47*, 45−48.

(9) Arnaiz, F. J.; Miranda, M. J. Microscale synthesis of UO2Cl2(OPPh3)2. *J. Chem. Educ.* **1998**, *75* (11), 1457−1458.

(10) Crawford, M. J.; Ellern, A.; Karaghiosoff, K.; Mayer, P.; Noth, H.; Suter, M. Synthesis and characterization of heavier dioxouranium-(VI) dihalides. *Inorg. Chem.* **2004**, *43* (22), 7120−7126.

(11) Haller, L. J. L.; Kaltsoyannis, N.; Sarsfield, M. J.; May, I.; Cornet, S. M.; Redmond, M. P.; Helliwell, M. A structural and theoretical investigation of equatorial cis and trans uranyl phosphinimine and uranyl phosphine oxide complexes UO2Cl2-(Cy3PNH)2 and UO2Cl2(Cy3PO)2. *Inorg. Chem.* **2007**, *46* (12), 4868−4875.

(12) Redmond, M. P.; Cornet, S. M.; Woodall, S. D.; Whittaker, D.; Collison, D.; Helliwell, M.; Natrajan, L. S. Probing the local coordination environment and nuclearity of uranyl(VI) complexes in non-aqueous media by emission spectroscopy. *Dalton. Trans.* **2011**, *40* (15), 3914−3926.

(13) Hashem, E.; McCabe, T.; Schulzke, C.; Baker, R. J. Synthesis, structure and photophysical properties of UO2 × 2(O═PPh3)2 (X = Cl, Br, I). *Dalton. Trans.* **2014**, *43* (3), 1125−1131.

(14) Hutschka, F.; Dedieu, A.; Troxler, L.; Wipff, G. Theoretical studies on the UO22+ and Sr2+ complexation by phosphoryl-containing O═PR3 ligands: QM ab initio calculations in the gas phase and MD FEP calculations in aqueous solution. *J. Phys. Chem. A* **1998**, *102* (21), 3773−3781.

(15) Arnaiz, F. J.; Miranda, M. J.; Aguado, R.; Mahia, J.; Maestro, M. A. Synthesis and molecular structure of the all-trans- and the trans-cis-UO2Br2(OAsPh3)2 isomers. *Polyhedron* **2001**, *20* (28), 3295−3299.

(16) Wang, C. Z.; Lan, J. H.; Zhao, Y. L.; Chai, Z. F.; Wei, Y. Z.; Shi, W. Q. Density functional theory studies of UO22+ and NpO2+ complexes with carbamoylmethylphosphine oxide ligands. *Inorg. Chem.* **2013**, *52* (1), 196−203.

(17) Vats, B. G.; Kannan, S.; Parvathi, K.; Maity, D. K.; Drew, M. G. B. Steric effects in complexes of diphenyl(2-pyridyl)phosphine oxide with the uranyl ion. Synthetic, structural and theoretical studies. *Polyhedron* **2015**, *89*, 116−121.

(18) Raychaudhuri, D.; Gopakumar, G.; Nagarajan, S.; Brahmmananda Rao, C. V. S. On the nature of the carbonyl versus phosphoryl binding in uranyl nitrate complexes. *J. Phys. Chem. A* **2020**, *124* (38), 7805−7815.

(19) Denning, R. G. Electronic-structure and bonding in actinyl ions. *Struct. Bonding (Berlin)* **1992**, *79*, 215−276.

(20) Denning, R. G.; Green, J. C.; Hutchings, T. E.; Dallera, C.; Tagliaferri, A.; Giarda, K.; Brookes, N. B.; Braicovich, L. Covalency in the uranyl ion: A polarized X-ray spectroscopic study. *J. Chem. Phys.* **2002**, *117* (17), 8008−8020.

(21) Denning, R. G. Electronic structure and bonding in actinyl ions and their analogs. *J. Phys. Chem. A* **2007**, *111* (20), 4125−4143.

(22) Cowie, B. E.; Purkis, J. M.; Austin, J.; Love, J. B.; Arnold, P. L. Thermal and photochemical reduction and functionalization chemistry of the uranyl dication, [U(VI)O2]2+. *Chem. Rev.* **2019**, *119* (18), 10595−10637.

(23) Dau, P. D.; Su, J.; Liu, H.-T.; Huang, D.-L.; Li, J.; Wang, L.-S. Photoelectron spectroscopy and the electronic structure of the uranyl tetrachloride dianion: UO2Cl42-. *J. Chem. Phys.* **2012**, *137* (6), No. 064315.

(24) Su, J.; Dau, P. D.; Qiu, Y. H.; Liu, H. T.; Xu, C. F.; Huang, D. L.; Wang, L. S.; Li, J. Probing the electronic structure and chemical bonding in tricoordinate uranyl complexes UO2 × 3- (X = F, Cl, Br, I): Competition between Coulomb repulsion and U-X bonding. *Inorg. Chem.* **2013**, *52* (11), 6617−6626.

(25) Liu, J. B.; Chen, G. P.; Huang, W.; Clark, D. L.; Schwarz, W. H. E.; Li, J. Bonding trends across the series of tricarbonato-actinyl anions (AnO2)(CO3)3(4-) (An = U-Cm): the plutonium turn. *Dalton. Trans.* **2017**, *46* (8), 2542−2550.

(26) Odoh, S. O.; Schreckenbach, G. DFT study of uranyl peroxo complexes with H2O, F-, OH-, CO32-, and NO3-. *Inorg. Chem.* **2013**, *52* (9), 5590−5602.

(27) Choppin, G. R. Covalency in f element bonds. *J. Alloys Compd.* **2002**, *344* (1−2), 55−59.

(28) Neidig, M. L.; Clark, D. L.; Martin, R. L. Covalency in f element complexes. *Coord. Chem. Rev.* **2013**, *257* (2), 394−406.

(29) Solomon, E. I.; Hedman, B.; Hodgson, K. O.; Dey, A.; Szilagyi, R. K. Ligand K-edge X-ray absorption spectroscopy: covalency of ligand-metal bonds. *Coord. Chem. Rev.* **2005**, *249* (1−2), 97−129.

(30) Tenderholt, A. L.; Wang, J.-J.; Szilagyi, R. K.; Holm, R. H.; Hodgson, K. O.; Hedman, B.; Solomon, E. I. Sulfur K-Edge X-ray Absorption Spectroscopy and Density Functional Calculations on Mo(IV) and Mo(VI)═O Bis-dithiolenes: Insights into the Mechanism of Oxo Transfer in DMSO Reductase and Related Functional Analogues. *J. Am. Chem. Soc.* **2010**, *132* (24), 8359−8371.

(31) Ha, Y.; Tenderholt, A. L.; Holm, R. H.; Hedman, B.; Hodgson, K. O.; Solomon, E. I. Sulfur K-Edge X-ray Absorption Spectroscopy and Density Functional Theory Calculations on Monooxo Mo-IV and Bisoxo Mo-VI Bis-dithiolenes: Insights into the Mechanism of Oxo Transfer in Sulfite Oxidase and Its Relation to the Mechanism of DMSO Reductase. *J. Am. Chem. Soc.* **2014**, *136* (25), 9094−9105.

(32) Ha, Y.; Arnold, A. R.; Nuñez, N. N.; Bartels, P. L.; Zhou, A.; David, S. S.; Barton, J. K.; Hedman, B.; Hodgson, K. O.; Solomon, E. I. Sulfur K-Edge XAS Studies of the Effect of DNA Binding on the [Fe4S4] Site in EndoIII and MutY. *J. Am. Chem. Soc.* **2017**, *139* (33), 11434−11442.

(33) Kozimor, S. A.; Yang, P.; Batista, E. R.; Boland, K. S.; Burns, C. J.; Christensen, C. N.; Clark, D. L.; Conradson, S. D.; Hay, P. J.; Lezama, J. S.; Martin, R. L.; Schwarz, D. E.; Wilkerson, M. P.; Wolfsberg, L. E. Covalency trends in group IV metallocene dichlorides. Chlorine K-edge X-ray absorption spectroscopy and time dependent-density functional theory. *Inorg. Chem.* **2008**, *47* (12), 5365−5371.

(34) Kozimor, S. A.; Yang, P.; Batista, E. R.; Boland, K. S.; Burns, C. J.; Clark, D. L.; Conradson, S. D.; Martin, R. L.; Wilkerson, M. P.; Wolfsberg, L. E. Trends in covalency for d- and f element metallocene dichlorides identified using chlorine K-edge X-ray absorption spectroscopy and time-dependent density functional theory. *J. Am. Chem. Soc.* **2009**, *131* (34), 12125−12136.

(35) Minasian, S. G.; Keith, J. M.; Batista, E. R.; Boland, K. S.; Clark, D. L.; Conradson, S. D.; Kozimor, S. A.; Martin, R. L.; Schwarz, D. E.; Shuh, D. K.; Wagner, G. L.; Wilkerson, M. P.; Wolfsberg, L. E.; Yang, P. Determining relative f and d orbital contributions to M-Cl covalency in MCl62- (M = Ti, Zr, Hf, U) and UOCl5- using Cl K-edge X-ray absorption spectroscopy and time-dependent density functional theory. *J. Am. Chem. Soc.* **2012**, *134* (12), 5586−5597.

https://doi.org/10.1021/acs.inorgchem.1c02236
Inorg. Chem. XXXX, XXX, XXX−XXX

(36) Löble, M. W.; Keith, J. M.; Altman, A. B.; Stieber, S. C. E.; Batista, E. R.; Boland, K. S.; Conradson, S. D.; Clark, D. L.; Lezama Pacheco, J.; Kozimor, S. A.; et al. Covalency in lanthanides. An X-ray absorption spectroscopy and density functional theory study of LnCl(6)(x-) (x = 3, 2). *J. Am. Chem. Soc.* **2015**, *137* (7), 2506−2523.
(37) Spencer, L. P.; Yang, P.; Minasian, S. G.; Jilek, R. E.; Batista, E. R.; Boland, K. S.; Boncella, J. M.; Conradson, S. D.; Clark, D. L.; Hayton, T. W.; Kozimor, S. A.; Martin, R. L.; MacInnes, M. M.; Olson, A. C.; Scott, B. L.; Shuh, D. K.; Wilkerson, M. P. Tetrahalide complexes of the U(NR)2(2+) ion: Synthesis, theory, and chlorine K-edge X-ray absorption spectroscopy. *J. Am. Chem. Soc.* **2013**, *135* (6), 2279−2290.
(38) Cross, J. N.; Su, J.; Batista, E. R.; Cary, S. K.; Evans, W. J.; Kozimor, S. A.; Mocko, V.; Scott, B. L.; Stein, B. W.; Windorff, C. J.; Yang, P. Covalency in americium(III) hexachloride. *J. Am. Chem. Soc.* **2017**, *139* (25), 8667−8677.
(39) Su, J.; Batista, E. R.; Boland, K. S.; Bone, S. E.; Bradley, J. A.; Cary, S. K.; Clark, D. L.; Conradson, S. D.; Ditter, A. S.; Kaltsoyannis, N.; Keith, J. M.; Kerridge, A.; Kozimor, S. A.; Löble, M. W.; Martin, R. L.; Minasian, S. G.; Mocko, V.; La Pierre, H. S.; Seidler, G. T.; Shuh, D. K.; Wilkerson, M. P.; Wolfsberg, L. E.; Yang, P. Energy-degeneracy-driven covalency in actinide bonding. *J. Am. Chem. Soc.* **2018**, *140* (51), 17977−17984.
(40) Minasian, S. G.; Keith, J. M.; Batista, E. R.; Boland, K. S.; Kozimor, S. A.; Martin, R. L.; Shuh, D. K.; Tyliszczak, T.; Vernon, L. J. Carbon K-edge X-ray absorption spectroscopy and time-dependent density functional theory examination of metal-carbon bonding in metallocene dichlorides. *J. Am. Chem. Soc.* **2013**, *135* (39), 14731−14740.
(41) Minasian, S. G.; Keith, J. M.; Batista, E. R.; Boland, K. S.; Clark, D. L.; Kozimor, S. A.; Martin, R. L.; Shuh, D. K.; Tyliszczak, T. New evidence for 5f covalency in actinocenes determined from carbon K-edge XAS and electronic structure theory. *Chemical Science* **2014**, *5* (1), 351−359.
(42) Smiles, D. E.; Batista, E. R.; Booth, C. H.; Clark, D. L.; Keith, J. M.; Kozimor, S. A.; Martin, R. L.; Minasian, S. G.; Shuh, D. K.; Stieber, S. C. E.; Tyliszczak, T. The duality of electron localization and covalency in lanthanide and actinide metallocenes. *Chemical Science* **2020**, *11* (10), 2796−2809.
(43) Pemmaraju, C. D.; Copping, R.; Wang, S. A.; Janousch, M.; Teat, S. J.; Tyliszcak, T.; Canning, A.; Shuh, D. K.; Prendergast, D. Bonding and charge transfer in nitrogen-donor uranyl complexes: Insights from NEXAFS spectra. *Inorg. Chem.* **2014**, *53* (21), 11415−11425.
(44) Wen, X. D.; Löble, M. W.; Batista, E. R.; Bauer, E.; Boland, K. S.; Burrell, A. K.; Conradson, S. D.; Daly, S. R.; Kozimor, S. A.; Minasian, S. G.; Martin, R. L.; McCleskey, T. M.; Scott, B. L.; Shuh, D. K.; Tyliszczak, T. Electronic structure and O K-edge XAS spectroscopy of U3O8. *J. Electron Spectrosc. Relat. Phenom.* **2014**, *194*, 81−87.
(45) Altman, A. B.; Pacold, J. I.; Wang, J.; Lukens, W. W.; Minasian, S. G. Evidence for 5d sigma and 5d pi covalency in lanthanide sesquioxides from oxygen K-edge X-ray absorption spectroscopy. *Dalton. Trans.* **2016**, *45* (24), 9948−9961.
(46) Minasian, S. G.; Batista, E. R.; Booth, C. H.; Clark, D. L.; Keith, J. M.; Kozimor, S. A.; Lukens, W. W.; Martin, R. L.; Shuh, D. K.; Stieber, S. C. E.; Tylisczcak, T.; Wen, X. D. Quantitative evidence for lanthanide-oxygen orbital mixing in CeO2, PrO2, and TbO2. *J. Am. Chem. Soc.* **2017**, *139* (49), 18052−18064.
(47) Frati, F.; Hunault, M. O. J. Y.; de Groot, F. M. F. Oxygen K-edge X-ray absorption spectra. *Chem. Rev.* **2020**, *120* (9), 4056−4110.
(48) Agostini, G.; Giacometti, G.; Clemente, D. A.; Vicentini, M. Crystal and molecular-structure of uranyl-nitrate trimethylphosphate. *Inorg. Chim. Acta* **1982**, *62* (2), 237−240.
(49) Burns, J. H.; Brown, G. M.; Ryan, R. R. Structure of dinitratodioxobis(triisobutyl phosphate)uranium(VI) at 139 K. *Acta Crystallogr., Sect. C: Cryst. Struct. Commun.* **1985**, *41* (OCT), 1446−1448.
(50) John, G. H.; May, I.; Sarsfield, M. J.; Collison, D.; Helliwell, M. Dimeric uranyl complexes with bridging perrhenates. *Dalton. Trans.* **2007**, *16*, 1603−1610.
(51) Bandoli, G.; Bortolozzo, G.; Clemente, D. A.; Croatto, U.; Panattoni, C. Crystal and molecular structure of triphenylphosphine oxide. *J. Chem. Soc. A* **1970**, *17*, 2778−2780.
(52) Brock, C. P.; Schweizer, W. B. Internal molecular-motion of triphenylphosphine oxide - analysis of atomic displacement parameters for orthorhombic and monoclinic crystal modifications at 100-K and 150-K. *J. Am. Chem. Soc.* **1985**, *107* (24), 6964−6970.
(53) Etter, M. C.; Baures, P. W. Triphenylphosphine oxide as a crystallization aid. *J. Am. Chem. Soc.* **1988**, *110* (2), 639−640.
(54) Davies, J. A.; Dutremez, S.; Pinkerton, A. A. Solid-state phosphorus-31 NMR and X-ray crystallographic studies of tertiary phosphines and their derivatives. *Inorg. Chem.* **1991**, *30* (10), 2380−2387.
(55) Alfarhan, K. A. Crystal-structure of triphenylphosphine oxide. *J. Crystallogr. Spectrosc. Res.* **1992**, *22* (6), 687−689.
(56) Thomas, J. A.; Hamor, T. A. Structure of orthorhombic triphenylphosphine oxide - A redetermination at room-temperature. *Acta Crystallogr., Sect. C: Cryst. Struct. Commun.* **1993**, *49*, 355−357.
(57) Orama, O.; Koskinen, J. T. Ethyldiphenylphosphine oxide, (C6H5)2(C2H5)PO. *Acta Crystallogr., Sect. C: Cryst. Struct. Commun.* **1994**, *50*, 608−609.
(58) Hilliard, C. R.; Bhuvanesh, N.; Gladysz, J. A.; Bluemel, J. Synthesis, purification, and characterization of phosphine oxides and their hydrogen peroxide adducts. *Dalton. Trans.* **2012**, *41* (6), 1742−1754.
(59) Hilliard, C. R.; Kharel, S.; Cluff, K. J.; Bhuvanesh, N.; Gladysz, J. A.; Bluemel, J. Structures and Unexpected Dynamic Properties of Phosphine Oxides Adsorbed on Silica Surfaces. *Chem. - Eur. J.* **2014**, *20* (52), 17292−17295.
(60) Donahue, C. M.; McCollom, S. P.; Forrest, C. M.; Blake, A. V.; Bellott, B. J.; Keith, J. M.; Daly, S. R. Impact of Coordination Geometry, Bite Angle, and Trans Influence on Metal-Ligand Covalency in Phenyl-Substituted Phosphine Complexes of Ni and Pd. *Inorg. Chem.* **2015**, *54* (12), 5646−5659.
(61) Lee, K.; Wei, H.; Blake, A. V.; Donahue, C. M.; Keith, J. M.; Daly, S. R. Ligand K-edge XAS, DFT, and TDDFT analysis of pincer linker variations in Rh(I) PNP complexes: reactivity insights from electronic structure. *Dalton. Trans.* **2016**, *45* (24), 9774−9785.
(62) Donahue, C. M.; Daly, S. R. Ligand K-Edge XAS Studies of Metal-Phosphorus Bonds: Applications, Limitations, and Opportunities. *Comments Inorg. Chem.* **2018**, *38* (2), 54−78.
(63) Lee, K.; Blake, A. V.; Donahue, C. M.; Spielvogel, K. D.; Bellott, B. J.; Daly, S. R. Quantifying the Interdependence of Metal-Ligand Covalency and Bond Distance using Ligand K-edge XAS. *Angew. Chem., Int. Ed.* **2019**, *58*, 12451−12455.
(64) Lee, K.; Wei, H.; Blake, A. V.; Donahue, C. M.; Keith, J. M.; Daly, S. R. Measurement of Diphosphine sigma-Donor and pi-Acceptor Properties in d(0) Titanium Complexes Using Ligand K-Edge XAS and TDDFT. *Inorg. Chem.* **2018**, *57* (16), 10277−10286.
(65) Blake, A. V.; Wei, H. C.; Lee, K.; Donahue, C. M.; Keith, J. M.; Daly, S. R. Solution and Solid-State Ligand K-Edge XAS Studies of PdCl2 Diphosphine Complexes with Phenyl and Cyclohexyl Substituents. *Eur. J. Inorg. Chem.* **2018**, *2018* (20−21), 2267−2276.
(66) Fortier, S.; Hayton, T. W. Oxo ligand functionalization in the uranyl ion (UO22+). *Coord. Chem. Rev.* **2010**, *254* (3−4), 197−214.
(67) Fillaux, C.; Guillaumont, D.; Berthet, J.-C.; Copping, R.; Shuh, D. K.; Tyliszczak, T.; Auwer, C. D. Investigating the electronic structure and bonding in uranyl compounds by combining NEXAFS spectroscopy and quantum chemistry. *Phys. Chem. Chem. Phys.* **2010**, *12* (42), 14253−14262.
(68) Martin, R. L.; Shirley, D. A. Many electron theory of electron emission. In *Electron Spectroscopy: Theory, Techniques and Applications*; Brundle, C. R., Baker, A. D., Eds.; Academic Press: London, 1977; Vol. *1*, pp 75−117.
(69) Segala, M.; Chong, D. P. K-shell core-electron binding energies for phosphorus- and sulfur-containing molecules calculated by density

https://doi.org/10.1021/acs.inorgchem.1c02236
Inorg. Chem. XXXX, XXX, XXX−XXX

functional theory. *J. Electron Spectrosc. Relat. Phenom.* **2010**, *182* (3), 141−144.
(70) Barton, R. L.; Gardenghi, D. J.; Stolte, W. C.; Szilagyi, R. K. Multiedge X-ray absorption spectroscopy Part II: XANES analysis of bridging and terminal chlorides in hexachlorodipalladate(II) complex. *J. Phys. Chem. A* **2015**, *119* (22), 5579−5586.
(71) McLaughlin, B. M.; Ballance, C. P.; Bowen, K. P.; Gardenghi, D. J.; Stolte, W. C. High precision k-shell photoabsorption cross sections for atomic oxygen: Experiment and theory. *Astrophys. J., Lett.* **2013**, *779* (2), L31.
(72) Stöhr, J. *NEXAFS Spectroscopy*. Springer-Verlag: Berlin, 1992.
(73) Groot, F.d.; Kotani, A. *Core Level Spectroscopy of Solids*; CRC Press, 2008.
(74) Neese, F.; Hedman, B.; Hodgson, K. O.; Solomon, E. I. Relationship between the dipole strength of ligand pre-edge transitions and metal-ligand covalency. *Inorg. Chem.* **1999**, *38* (21), 4854−4860.
(75) de Sahb, C.; Watson, L. A.; Nadas, J.; Hay, B. P. Design Criteria for Polyazine Extractants To Separate AnIII from LnIII. *Inorg. Chem.* **2013**, *52* (18), 10632−10642.
(76) Pham, T. A.; Altman, A. B.; Stieber, S. C. E.; Booth, C. H.; Kozimor, S. A.; Lukens, W. W.; Olive, D. T.; Tyliszczak, T.; Wang, J.; Minasian, S. G.; Raymond, K. N. A Macrocyclic Chelator That Selectively Binds Ln4+ over Ln3+ by a Factor of 1029. *Inorg. Chem.* **2016**, *55* (20), 9989−10002.
(77) Hudson, M. J.; Harwood, L. M.; Laventine, D. M.; Lewis, F. W. Use of Soft Heterocyclic N-Donor Ligands To Separate Actinides and Lanthanides. *Inorg. Chem.* **2013**, *52* (7), 3414−3428.
(78) Manna, D.; Ghanty, T. K. Complexation behavior of trivalent actinides and lanthanides with 1,10-phenanthroline-2,9-dicarboxylic acid based ligands: insight from density functional theory. *Phys. Chem. Chem. Phys.* **2012**, *14* (31), 11060−11069.
(79) Roy, L. E.; Bridges, N. J.; Martin, L. R. Theoretical insights into covalency driven f element separations. *Dalton. Trans.* **2013**, *42* (7), 2636−2642.
(80) Xiao, C.-L.; Wang, C.-Z.; Yuan, L.-Y.; Li, B.; He, H.; Wang, S.; Zhao, Y.-L.; Chai, Z.-F.; Shi, W.-Q. Excellent Selectivity for Actinides with a Tetradentate 2,9-Diamide-1,10-Phenanthroline Ligand in Highly Acidic Solution: A Hard-Soft Donor Combined Strategy. *Inorg. Chem.* **2014**, *53* (3), 1712−1720.
(81) Xiao, C.-L.; Wu, Q.-Y.; Wang, C.-Z.; Zhao, Y.-L.; Chai, Z.-F.; Shi, W.-Q. Quantum Chemistry Study of Uranium(VI), Neptunium-(V), and Plutonium(IV,VI) Complexes with Preorganized Tetradentate Phenanthrolineamide Ligands. *Inorg. Chem.* **2014**, *53* (20), 10846−10853.
(82) Surbella, R. G., III; Andrews, M. B.; Cahill, C. L. Self assembly of UO2 × 4(2-) (X = Cl, Br) dianions with gamma substituted pyridinium cations: Structural systematics and fluorescence properties. *J. Solid State Chem.* **2016**, *236*, 257−271.
(83) Crawford, M. J.; Mayer, P. Synthesis, structural and computational investigations of UO2I42-: A structurally characterized U(VI)-I anion. *Inorg. Chem.* **2005**, *44* (16), 5547−5549.
(84) Sheldrick, G. M. A short history of SHELX. *Acta Crystallogr., Sect. A: Found. Crystallogr.* **2008**, *64*, 112−122.
(85) Dolomanov, O. V.; Bourhis, L. J.; Gildea, R. J.; Howard, J. A. K.; Puschmann, H. OLEX2: a complete structure solution, refinement and analysis program. *J. Appl. Crystallogr.* **2009**, *42*, 339−341.
(86) Ren, G. X.; Zhang, N.; Feng, X. F.; Zhang, H.; Yu, P. F.; Zheng, S.; Zhou, D.; Tian, Z. W.; Liu, X. S. Photon-in/photon-out endstation for studies of energy materials at beamline 02B02 of Shanghai Synchrotron Radiation Facility. *Chin. Phys. B* **2020**, *29* (1), No. 016101.
(87) Zheng, L.; Zhao, Y. D.; Tang, K.; Ma, C. Y.; Hong, C. H.; Han, Y.; Cui, M. Q.; Guo, Z. Y. A new experiment station on beamline 4B7A at Beijing Synchrotron Radiation Facility. *Spectrochim. Acta, Part B* **2014**, *101*, 1−5.
(88) Ravel, B.; Newville, M. ATHENA, ARTEMIS, HEPHAESTUS: data analysis for X-ray absorption spectroscopy using IFEFFIT. *J. Synchrotron Radiat.* **2005**, *12*, 537−541.
(89) George, G. N. *EDG_FIT*; Stanford Synchrotron Radiation Laboratory, Stanford Linear Accelerator Center, Stanford University: Stanford, CA, 2001.
(90) Baerends, E. J.; Ziegler, T.; Autschbach, J.; Bashford, D.; Bérces, A.; Bickelhaupt, F.M.; Bo, C.; Boerrigter, P.M.; Cavallo, L.; Chong, D.P. et al. *ADF2019*; SCM, Theoretical Chemistry, Vrije Universiteit, Amsterdam, The Netherlands, 2019. https://www.scm.com/product/adf/.
(91) te Velde, G.; Bickelhaupt, F. M.; Baerends, E. J.; Fonseca Guerra, C.; van Gisbergen, S. J. A.; Snijders, J. G.; Ziegler, T. Chemistry with ADF. *J. Comput. Chem.* **2001**, *22* (9), 931−967.
(92) Becke, A. D. Density-functional exchange-energy approximation with correct asymptotic-behavior. *Phys. Rev. A: At., Mol., Opt. Phys.* **1988**, *38* (6), 3098−3100.
(93) Lee, C. T.; Yang, W. T.; Parr, R. G. Development of the Colle-Salvetti correlation-energy formula into a functional of the electron-density. *Phys. Rev. B: Condens. Matter Mater. Phys.* **1988**, *37* (2), 785−789.
(94) Faas, S.; Snijders, J. G.; Vanlenthe, J. H.; Vanlenthe, E.; Baerends, E. J. The ZORA formalism applied to the Dirac-Fock equation. *Chem. Phys. Lett.* **1995**, *246* (6), 632−640.
(95) Grimme, S. A simplified Tamm-Dancoff density functional approach for the electronic excitation spectra of very large molecules. *J. Chem. Phys.* **2013**, *138* (24), 244104.
(96) Bannwarth, C.; Grimme, S. A simplified time-dependent density functional theory approach for electronic ultraviolet and circular dichroism spectra of very large molecules. *Comput. Theor. Chem.* **2014**, *1040*, 45−53.

https://doi.org/10.1021/acs.inorgchem.1c02236
Inorg. Chem. XXXX, XXX, XXX−XXX